Experimental demonstration of ultrasensitive sensing with terahertz metamaterial absorbers: A comparison with the metasurfaces

Cong, Longqing; Tan, Siyu; Yahiaoui, Riad; Yan, Fengping; Zhang, Weili; Singh, Ranjan

2015

Cong, L., Tan, S., Yahiaoui, R., Yan, F., Zhang, W., & Singh, R. (2015). Experimental demonstration of ultrasensitive sensing with terahertz metamaterial absorbers: A comparison with the metasurfaces. Applied Physics Letters, 106(3), 031107-.

https://hdl.handle.net/10356/107143

https://doi.org/10.1063/1.4906109

AIP | Applied Physics Letters

Experimental demonstration of ultrasensitive sensing with terahertz metamaterial absorbers: A comparison with the metasurfaces

Longqing Cong, Siyu Tan, Riad Yahiaoui, Fengping Yan, Weili Zhang, and Ranjan Singh

Citation: Applied Physics Letters **106**, 031107 (2015); doi: 10.1063/1.4906109
View online: http://dx.doi.org/10.1063/1.4906109
View Table of Contents: http://scitation.aip.org/content/aip/journal/apl/106/3?ver=pdfcov
Published by the AIP Publishing

Experimental demonstration of ultrasensitive sensing with terahertz metamaterial absorbers: A comparison with the metasurfaces

Longqing Cong,[1,2] Siyu Tan,[3,4] Riad Yahiaoui,[5] Fengping Yan,[4] Weili Zhang,[3] and Ranjan Singh[1,2,a)]

[1]*Division of Physics and Applied Physics, School of Physical and Mathematical Sciences, Nanyang Technological University, Singapore 637371, Singapore*
[2]*Centre for Disruptive Photonic Technologies, School of Physical and Mathematical Sciences, Nanyang Technological University, Singapore 637371, Singapore*
[3]*School of Electrical Engineering and Computer Science, Oklahoma State University, Stillwater, Oklahoma 87074, USA*
[4]*Key Lab of All Optical Network and Advanced Telecommunication Network of EMC, Institute of Lightwave Technology, Beijing Jiaotong University, Beijing 100044, People's Republic of China*
[5]*XLIM, Limoges University, CNRS, UMR 7252, 7 rue Jules Vallès, F-19100 Brive, France*

(Received 9 December 2014; accepted 2 January 2015; published online 20 January 2015)

Planar metasurfaces and plasmonic resonators have shown great promise for sensing applications across the electromagnetic domain ranging from the microwaves to the optical frequencies. However, these sensors suffer from lower figure of merit and sensitivity due to the radiative and the non-radiative loss channels in the plasmonic metamaterial systems. We demonstrate a metamaterial absorber based ultrasensitive sensing scheme at the terahertz frequencies with significantly enhanced sensitivity and an order of magnitude higher figure of merit compared to planar metasurfaces. Magnetic and electric resonant field enhancement in the impedance matched absorber cavity enables stronger interaction with the dielectric analyte. This finding opens up opportunities for perfect metamaterial absorbers to be applied as efficient sensors in the finger print region of the electromagnetic spectrum with several organic, explosive, and bio-molecules that have unique spectral signature at the terahertz frequencies. © *2015 AIP Publishing LLC*.
[http://dx.doi.org/10.1063/1.4906109]

The quest to bridge the terahertz (THz) gap in the electromagnetic spectrum has ushered enormous amount of research activities in the recent years.[1–5] With the nonionizing property of the so called "T-rays," the THz devices have attracted tremendous attention due to the broad applications in imaging, remote sensing, astronomical radiation detection, high resolution spectroscopy, and biomedical analytics.[6–11] In the recent times, artificially designed metamaterial devices[12–14] have emerged as an important tool to manipulate electromagnetic waves at the subwavelength scales due to the artificially engineered optical properties based on a periodic array of unit cells which are typically called "meta-atoms" and form the basis of many fascinating and exotic effects like negative refraction,[15,16] perfect lenses,[17] and cloaking.[18] Metamaterials and plasmonic based devices have also shown significant applications in chemical and biomedical sensing,[19] surface enhanced spectroscopy,[20] and near-field scanning optical microscopy.[21] The collective excitation of subwavelength metamaterial and plasmonic structures lead to localized electric and magnetic resonances which provide excellent platform for electromagnetic sensing.[22,23]

There has been several previous works that demonstrate sensing with planar metamaterial split ring resonators (SRRs).[24–34] However, either the sensitivity or the figure of merit (FoM) of such planar metamaterial sensors is relatively lower due to the low quality factor resonances caused by the losses[35] and the lack of strong electromagnetic interaction.[36,37] The substrate with relatively higher permittivity usually bounds most of electric field flux in the capacitive gap of the SRR that results in a weaker interaction of the analyte with the resonant electric field. Perfect metamaterial absorbers (PMAs) have emerged as strong candidates for absorbing electromagnetic waves,[2,38–46] which are typically three layered structures that consist of a micro/nanofabricated planar metasurface layer, a dielectric spacer, and a ground plane layer in the direction of propagation. It has been recently shown that such a tri-layer configuration forms a Fabry-Perot (F-P) cavity and the absorption effect occurs due to the interference between the multiple reflection inside the cavity,[42,47,48] which leads to significant field trapping and enhancement. Additionally, the ground plane isolates the interaction between the metamaterial device and the substrate, eliminating the detrimental effect of electric field decay in typically high dielectric substrates. We exploit these two distinct features of a PMA for enhanced light matter interaction and demonstrate ultrasensitive thin-film sensing of dielectric analyte layer deposited on PMAs.

In this manuscript, we present two different PMA designs for sensing application through detailed experiment and simulation at the technologically relevant THz frequencies. Terahertz PMA based sensors could have potential applications due to the unique spectral signature behavior of several explosives and organic materials in the THz regime.[4] We also compare the performance of PMA sensors with planar metasurface sensors with identical resonator design where the PMA sensor shows much superior performance in

a)Email: ranjans@ntu.edu.sg

terms of sensitivity and the FoM. The significance of biosensing in THz domain lies in the fact that biomolecules have vibrational resonances in the THz domain such as bovine serum albumin.[49] The refractive index of biomolecules can vary from 1.4 to 1.6 in DNA and 1.6 to 2.0 in RNA and the rotational-vibrational degrees of freedom, binding state, degree of hydration, and conformation can all induce the detectable shifts of the absorber resonance frequency.

A cross shaped absorber (CSA) and its complementary cross shaped absorber (CCSA) design with 4-fold rotational symmetry was chosen to investigate the sensitivity in terms of the shift in resonance frequency of the reflection spectra and the FoM. As shown in Figs. 1(a) and 1(c), we designed CSA and CCSA unit cells with the length of cross shaped structure as $l = 130\ \mu$m, and width $w = 15\ \mu$m. We deposited 200 nm thick aluminum layer ($\sigma = 3.56 \times e^7$ S/m) for both the structured top layer and the bottom ground plane layer. The thickness of polyimide ($\varepsilon = 2.96 + 0.27i$) spacer in CSA was chosen to be $h = 18\ \mu$m ($h = 31\ \mu$m for CCSA) in order to match the impedance for perfect absorption. A silicon ($\varepsilon = 11.9 + 0.0476i$) substrate with thickness of 500 μm was used for fabrication. With the incident electric field and wave vector direction shown in Fig. 1, the resonant electric fringing field above the absorber surface and the resonant magnetic field is artistically illustrated in Fig. 1(e). These electric and magnetic fields play key roles in sensing analytes that fall in the vicinity of the PMA sensor; when the analytes with different refractive indices are deposited on the top surfaces of CSA and CCSA sensors, the redistribution of electric and magnetic fields lead to a strong modulation of the absorber resonance frequency and amplitude.[50]

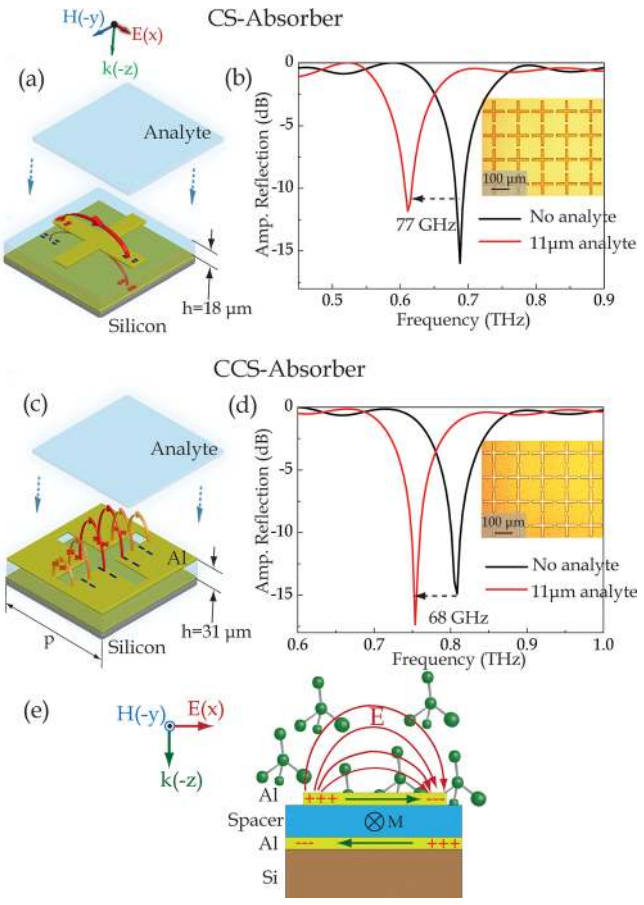

FIG. 1. (a) Cross shaped absorber (CSA) design and (b) amplitude reflection spectra of bare sample (black) and with 11 μm thick photoresist (red) (Inset: Image of the fabricated CSA sample). (c) Complementary cross shape absorber (CCSA) design and (d) amplitude reflection spectra of bare sample (black) and 11 μm thick photoresist (red) (Inset: Image of fabricated CCSA sample). (e) Artistic illustration of the electric and the magnetic field across the absorber sensor cross section with molecules from the top representing the analyte. Periodicity of CSA and CCSA is 150 μm by 150 μm, the arm width and length are 15 μm and 130 μm, respectively.

Terahertz time-domain spectroscopy system in the reflection mode was used to measure the response of the absorber sensor devices. Different thicknesses (t) of photoresist (refractive index, n = 1.6) were spun coated on the absorber surface, and their response was measured as shown in Figs. 1(b) and 1(d). The black curves represent the amplitude reflection spectra for the bare CSA and CCSA without any analyte coating. When 11 μm thick analyte was coated on the PMAs, we observed strong red shifts of 77 GHz and 68 GHz for CSA and CCSA sensors, respectively. A series of measurements were performed for both PMAs by coating photoresist of different thicknesses, $t = 0\ \mu$m, 3 μm, 6 μm, and 11 μm. The results consisting of different resonance frequency shift are shown as insets in Figs. 2(a) and 2(b). We define the frequency shift (FS) as $FS = (f_t - f_{\mathrm{Ref}})/f_{\mathrm{Ref}} \times 100\%$, where f_t is the resonance frequency of PMA with analyte thickness t and f_{Ref} as the resonance frequency of PMA without any analyte coating. We plotted the measured frequency shifts of the CSA and CCSA sensors for different analyte thicknesses in Figs. 2(a) and 2(b). A full-wave finite-element frequency-domain

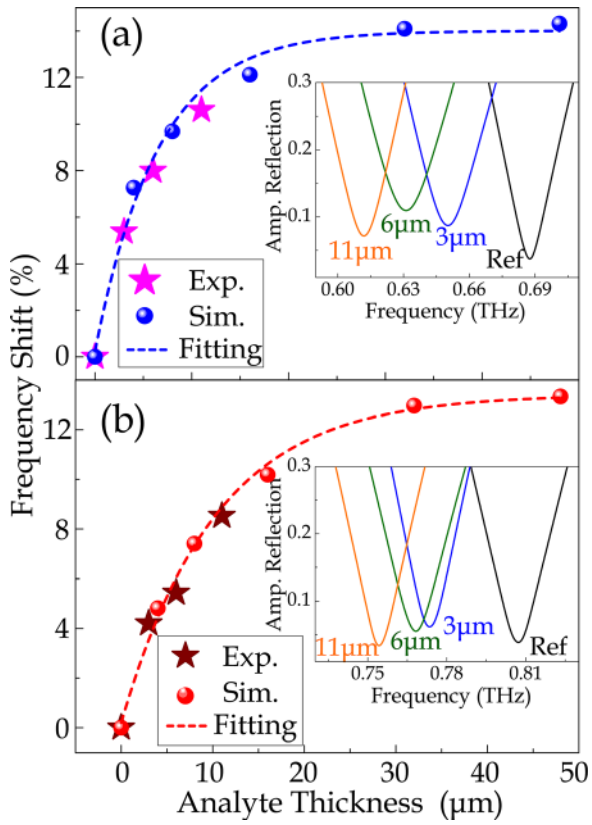

FIG. 2. Frequency shift versus the analyte thickness for (a) CSA and (b) CCSA with experimental (stars) and simulated (dots) data. The insets in (a) and (b) show the measured amplitude reflection spectra with varying analyte thicknesses for CSA and CCSA sensors. The dotted lines show the exponential fits to the experimental and simulation data.

Maxwell equation solver was used to simulate the results under conditions identical to the experiments have also been plotted in Figs. 2(a) and 2(b) along with the experimental results, where dashed lines show the exponential fits for the experimental and the simulated data indicating that the fringing fields decayed exponentially from the top surface of the PMA sensors. We observe from Figs. 2(a) and 2(b) that the experimental and simulated data matched reasonably well with the exponential functions. The fitting functions are described by $FS = 14.0 - 14.0e^{-\frac{t}{6.5}}$ and $FS = 13.4 - 13.4e^{-\frac{t}{10.3}}$, where the total frequency shift saturated at about 14.0% and 13.4% for CSA and CCSA sensors, respectively. The fringing fields determine the volume of the analyte required for the maximum frequency shift of the absorber resonance.

We also investigated the effect of different refractive index analyte on the absorber sensor through rigorous simulations. The absorber resonance frequency for a fixed analyte thickness while varying the refractive indices from n = 1.0 to n = 1.8 in incremental steps of 0.1 was calculated. The index dependent change in the resonance frequency for the CSA and the CCSA absorber sensors with two different analyte thicknesses of $t = 4\ \mu$m and $t = 48\ \mu$m was studied as shown in the insets of Figs. 3(a) and 3(d). The sensitivity (S) was defined as the slope of the linear fitting function. A significant increase in the sensitivity was observed when the analyte thickness was increased from $t = 4\ \mu$m to $t = 48\ \mu$m. The enhancement in sensitivity with the change in analyte thickness was plotted in Figs. 3(a) and 3(d). The exponential enhancement followed the forms $S = 24 - 18.7e^{-\frac{t}{8.9}}$ (CSA) and $S = 24 - 21.4e^{-\frac{t}{13.1}}$ (CCSA) with the highest sensitivities of 23.7% RIU^{-1} for CSA and 23.5% RIU^{-1} for CCSA sensor.

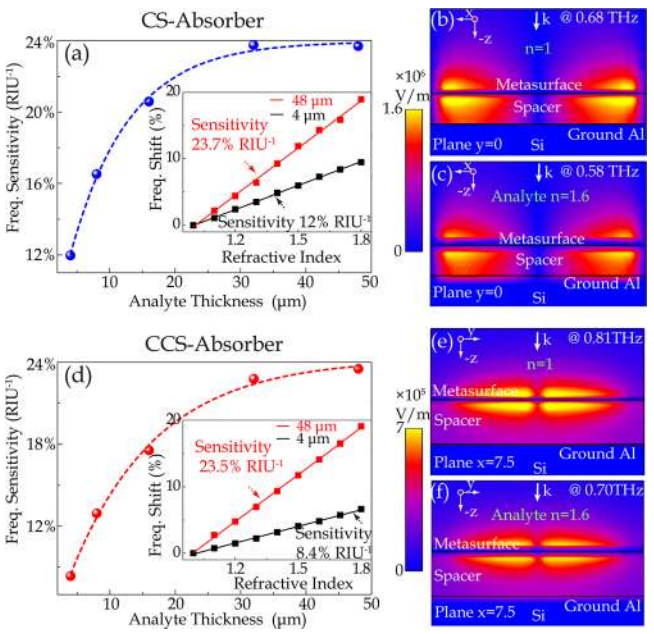

FIG. 3. The refractive index sensitivity versus the analyte thickness for (a) CSA and (d) CCSA. The insets in (a) and (d) show the refractive index sensitivity for 4 μm and 48 μm thick analyte. The electric field distribution in the z-direction in CSA absorber (b) without analyte and (c) with analyte at $y = 0$ cut-plane. The electric field distribution in the z-direction in CCSA absorber (e) without analyte and (f) with analyte at $x = 7.5\ \mu$m cut-plane.

In order to visualize the electric fields in the absorber structures, we simulated the electric field distribution in the x-z plane for CSA and y-z plane for CCSA as shown in Figs. 3(b) and 3(e), respectively. It clearly showed the electric field within the absorber structures as well as the spatial extent of the fringing fields. Figure 3(b) shows the longitudinal cross section of electric field distribution at $y = 0$ cut-plane for CSA, and Fig. 3(e) shows the cross-section at $y = 7.5\ \mu$m cut-plane for CCSA, where the centers of CSA and CCSA lie at $x = 0$ and $y = 0$ in the coordinate system. We observed the enhanced resonant fields in the spacer layer and above the structured resonator layer. The electric field in CSA was about twice stronger than that in the CCSA, which lead to higher sensitivity of thinner analyte layers (see the insets of Figs. 3(a) and 3(d)) in CSA as compared to CCSA. The extent of the spatial fringing field was also observed in both the absorbers. Figures 3(c) and 3(f) showed the electric fields in CSA and CCSA in the presence of 50 μm thick analyte layer with refractive index of 1.6. The fringing fields above the structured resonator layer and the fields in the absorber spacer layer were observed to be more confined in presence of the dielectric analyte layer in CSA and CCSA sensors.

The electric field resonant enhancement in absorbers originated from the multi pass light cycles within the F-P cavity that enabled a strong interaction between the analyte with the concentrated fields within the spacer layer as well as fringing fields that extend above the absorber surface. As observed in Figs. 3(b), 3(c), 3(e), and 3(f), the sensed analyte affects the field within the spacer region as well as above the absorber surface. Due to the presence of the analyte layer, the overall electric field was squeezed to a smaller spatial extent in the z-direction. Thus, the enhanced field in the absorber cavity (spacer layer) along with the fringing field above the absorber surface played a significant role in sensing of the analyte layers. This explained the highly sensitive nature of the PMA designs which has tremendous potential to be exploited for sensing applications.

For comparison, we also studied the sensing performance of the corresponding single layer planar metasurface fabricated directly on identical silicon substrate as used for the absorbers. The metasurface structures were identical to the top structured layer of both the absorber designs. We address the two planar metasurfaces as cross shaped metasurface (CSM) and the complementary cross shaped metasurface (CCSM) that correspond to the respective CSA and CCSA designs. Different thicknesses of the same photoresist (n = 1.6) was spun coat on top of the planar metasurfaces. The measured transmission spectra are shown in the insets of Figs. 4(a) and 4(d) for CSM and CCSM, respectively. The results show that the shift in the resonance frequency is not as strong as that in PMAs when the different thicknesses analyte were spun-coated on the metasurfaces. In case of planar metasurfaces, it is the electric field of the dipolar resonance and the fringing field above the metasurfaces that causes the shift in the resonance frequency. The simulated fields in the planar CSM and CCSM were shown in Figs. 4(b) and 4(e) (the same cut-planes as shown in Figs. 3(b) and 3(e) in case of absorbers). The electric field strengths in these planar metasurfaces have been found to be an order of magnitude

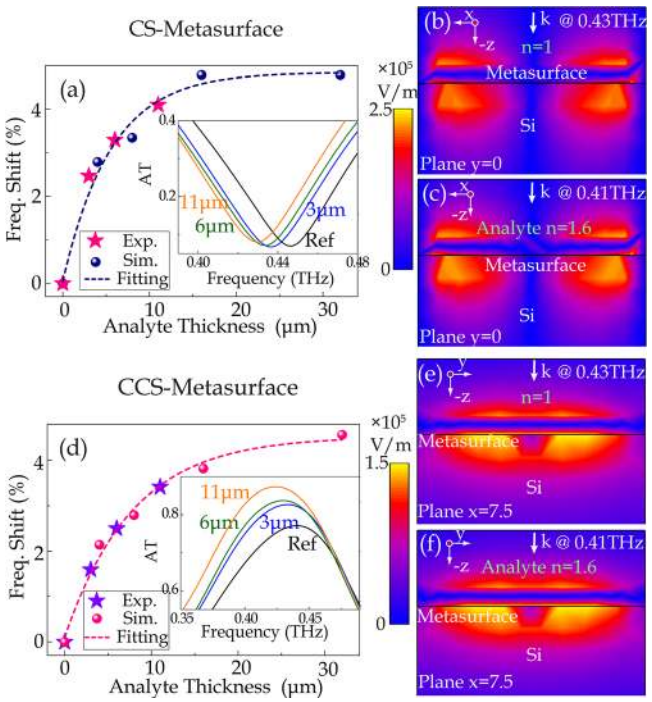

FIG. 4. Frequency shift versus the analyte thickness for (a) CSM and (d) CCSM with experimental (stars) and simulated (dots) data. The insets are the measured amplitude transmission spectra with varying analyte thicknesses. The electric field distribution in the z-direction in CSM (b) without analyte and (c) with analyte at $y = 0$ cut-plane. The electric field distribution in the z-direction in CCSM (e) without analyte and (f) with analyte at $x = 7.5\ \mu$m cut-plane.

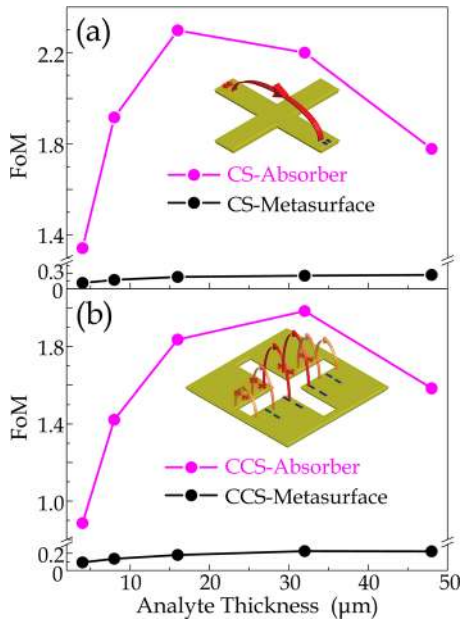

FIG. 5. Figure of merit of absorbers and planar metasurfaces for (a) cross shape and (b) complementary cross shape design.

TABLE I. Comparison between absorber and metasurface sensors.

	CS-absorber	CCS-absorber	CS-metasurface	CCS-metasurface
Q factor	11.6	11.0	3.32	2.69
FoM	2.30	1.98	0.27	0.22

weaker than their absorber counterparts. Apart from relatively weaker field strengths, there is no spacer layer in planar metasurfaces that would enhance the interaction time of the analyte with light that gets trapped in the F-P cavity formed by the three layered absorber structures. Thus, we found the absorbers to be much more efficient sensors as compared to the metasurfaces. Figures 4(c) and 4(f) showed the fields that penetrated the analyte layer (n = 1.6) deposited on top of the metasurface where the fields in the silicon substrate do not undergo any significant change. However, the fringing fields on top of the metasurfaces showed decrease in their spatial extent as they confined tightly in the analyte layer.

For a quantitative description of the sensing performance parameter, we estimated the FoM, defined here as $FoM = S \times Q$, where S represented the sensitivity and Q referred to the quality factor of the resonance. The calculated FoMs of absorbers (CSA, CCSA) and metasurfaces (CSM, CCSM) sensors are plotted in Fig. 5. The best FoM = 2.30 of the CSA sensor was observed at optimal analyte thickness of 16 μm and the best FoM = 1.98 of CCSA sensor was observed at optimal analyte thickness of 32 μm. The FoM values of absorber sensors have been found to be significantly higher than those of planar metasurface resonators. The detailed performance comparison in terms of Q factor and FoM for different sensors that we studied in this work is summarized in Table I.

In conclusion, we present two different engineered designs of perfect metamaterial absorbers as sensors in the THz regime and compared their performance with planar metasurface counterparts. We found that the sensitivity as well as the FoM values of the absorber sensors were significantly higher than the planar metasurfaces. The enhanced sensitivity of the absorbers is mainly attributed to the intense resonant electric and magnetic field enhancement in the absorber cavity and the fringing fields that extend out of the absorber plane. The field enhancement in metasurfaces is an order of magnitude lower than the absorbers which results in lower sensitivities and FoM values. In planar metasurface and plasmonic resonator structures, the sensing of analyte is performed by exploiting only the capacitive/dipolar fringing fields extending out of their surface planes. The absorber cavity offers an extremely attractive avenue for sensing analytes through their resonant electric as well as magnetic fields. Metamaterial absorber as a sensor would be an important addition to the device starved THz regime that holds significance due its finger print spectral range for several explosive, organic, and bio-molecules.

We thank G. Dayal and D. R. Chowdhury for fruitful discussions. L.C. and R.S. acknowledge NTU startup Grant No. M4081282 and MoE Tier 1 Grant No. M4011362 for funding of this research. This work was partially supported by the U.S. National Science Foundation (Grant No. ECCS-1232081).

[1]B. Ferguson and X.-C. Zhang, Nat. Mater. **1**, 26 (2002).
[2]H. Tao, N. I. Landy, C. M. Bingham, X. Zhang, R. D. Averitt, and W. J. Padilla, Opt. Express **16**, 7181 (2008).
[3]W. J. Padilla, A. J. Taylor, C. Highstrete, M. Lee, and R. D. Averitt, Phys. Rev. Lett. **96**, 107401 (2006).

[4]M. Tonouchi, Nat. Photonics **1**, 97 (2007).
[5]D. Grischkowsky, S. Keiding, M. v. Exter, and C. Fattinger, J. Opt. Soc. Am. B **7**, 2006 (1990).
[6]J. F. Federici, B. Schulkin, F. Huang, D. Gary, R. Barat, F. Oliveira, and D. Zimdars, Semicond. Sci. Technol. **20**, S266 (2005).
[7]L. Fekete, P. Kužel, H. Němec, F. Kadlec, A. Dejneka, J. Stuchlík, and A. Fejfar, Phys. Rev. B **79**, 115306 (2009).
[8]Z. D. Taylor, R. S. Singh, D. B. Bennett, P. Tewari, C. P. Kealey, N. Bajwa, M. O. Culjat, A. Stojadinovic, H. Lee, and J. Hubschman, IEEE Trans. Terahertz Sci. Technol. **1**, 201 (2011).
[9]T. Kippenberg, R. Holzwarth, and S. Diddams, Science **332**, 555 (2011).
[10]S. Komiyama, IEEE J. Sel. Top. Quantum Electron. **17**, 54 (2011).
[11]P. U. Jepsen, D. G. Cooke, and M. Koch, Laser Photonics Rev. **5**, 124 (2011).
[12]L. Cong, W. Cao, X. Zhang, Z. Tian, J. Gu, R. Singh, J. Han, and W. Zhang, Appl. Phys. Lett. **103**, 171107 (2013).
[13]L. Cong, N. Xu, J. Gu, R. Singh, J. Han, and W. Zhang, Laser Photonics Rev. **8**, 626 (2014).
[14]R. Singh, I. A. Al-Naib, Y. Yang, D. R. Chowdhury, W. Cao, C. Rockstuhl, T. Ozaki, R. Morandotti, and W. Zhang, Appl. Phys. Lett. **99**, 201107 (2011).
[15]D. R. Smith, W. J. Padilla, D. Vier, S. C. Nemat-Nasser, and S. Schultz, Phys. Rev. Lett. **84**, 4184 (2000).
[16]R. Yahiaoui, H. Němec, P. Kužel, F. Kadlec, C. Kadlec, and P. Mounaix, Opt. Lett. **34**, 3541 (2009).
[17]J. B. Pendry, Phys. Rev. Lett. **85**, 3966 (2000).
[18]J. B. Pendry, D. Schurig, and D. R. Smith, Science **312**, 1780 (2006).
[19]S. Lal, S. Link, and N. J. Halas, Nat. Photonics **1**, 641 (2007).
[20]S. Nie and S. R. Emory, Science **275**, 1102 (1997).
[21]R. C. Dunn, Chem. Rev. **99**, 2891 (1999).
[22]K. A. Willets and R. P. Van Duyne, Annu. Rev. Phys. Chem. **58**, 267 (2007).
[23]J. F. O'Hara, W. Withayachumnankul, and I. Al-Naib, J. Infrared, Millim., Terahertz Waves **33**, 245 (2012).
[24]C. Debus and P. H. Bolivar, Appl. Phys. Lett. **91**, 184102 (2007).
[25]S.-Y. Chiam, R. Singh, W. Zhang, and A. A. Bettiol, Appl. Phys. Lett. **97**, 191906 (2010).
[26]E. Cubukcu, S. Zhang, Y.-S. Park, G. Bartal, and X. Zhang, Appl. Phys. Lett. **95**, 043113 (2009).
[27]N. Liu, T. Weiss, M. Mesch, L. Langguth, U. Eigenthaler, M. Hirscher, C. Sönnichsen, and H. Giessen, Nano Lett. **10**, 1103 (2009).
[28]C. Wu, A. B. Khanikaev, R. Adato, N. Arju, A. A. Yanik, H. Altug, and G. Shvets, Nat. Mater. **11**, 69 (2012).
[29]J. Zhao, C. Zhang, P. V. Braun, and H. Giessen, Adv. Mater. **24**, OP247 (2012).
[30]J. F. O'Hara, R. Singh, I. Brener, E. Smirnova, J. Han, A. J. Taylor, and W. Zhang, Opt. Express **16**, 1786 (2008).
[31]H. Tao, L. R. Chieffo, M. A. Brenckle, S. M. Siebert, M. Liu, A. C. Strikwerda, K. Fan, D. L. Kaplan, X. Zhang, and R. D. Averitt, Adv. Mater. **23**, 3197 (2011).
[32]W. Withayachumnankul, H. Lin, K. Serita, C. M. Shah, S. Sriram, M. Bhaskaran, M. Tonouchi, C. Fumeaux, and D. Abbott, Opt. Express **20**, 3345 (2012).
[33]I. A. I. Al-Naib, C. Jansen, and M. Koch, Appl. Phys. Lett. **93**, 083507 (2008).
[34]R. Singh, W. Cao, I. Al-Naib, L. Cong, W. Withayachumnankul, and W. Zhang, Appl. Phys. Lett. **105**, 171101 (2014).
[35]R. Singh and N. Zheludev, Nat. Photonics **8**, 679 (2014).
[36]R. Singh, I. A. Al-Naib, M. Koch, and W. Zhang, Opt. Express **19**, 6312 (2011).
[37]R. Singh, I. Al-Naib, W. Cao, C. Rockstuhl, M. Koch, and W. Zhang, IEEE Trans. Terahertz Sci. Technol. **3**, 820 (2013).
[38]N. Landy, S. Sajuyigbe, J. Mock, D. Smith, and W. Padilla, Phys. Rev. Lett. **100**, 207402 (2008).
[39]N. Liu, M. Mesch, T. Weiss, M. Hentschel, and H. Giessen, Nano Lett. **10**, 2342 (2010).
[40]F. Cheng, X. Yang, and J. Gao, Opt. Lett. **39**, 3185 (2014).
[41]K. Aydin, V. E. Ferry, R. M. Briggs, and H. A. Atwater, Nat. Commun. **2**, 517 (2011).
[42]J. Zhou, H.-T. Chen, T. Koschny, A. K. Azad, A. J. Taylor, C. M. Soukoulis, and J. F. O'Hara, preprint arXiv:1111.0343 (2011).
[43]C. Wu, I. B. Neuner, G. Shvets, J. John, A. Milder, B. Zollars, and S. Savoy, Phys. Rev. B **84**, 075102 (2011).
[44]G. Dayal and S. A. Ramakrishna, Opt. Lett. **38**, 272 (2013).
[45]X. Shen, Y. Yang, Y. Zang, J. Gu, J. Han, W. Zhang, and T. J. Cui, Appl. Phys. Lett. **101**, 154102 (2012).
[46]R. Yahiaoui, J. P. Guillet, F. de Miollis, and P. Mounaix, Opt. Lett. **38**, 4988 (2013).
[47]H.-T. Chen, Opt. Express **20**, 7165 (2012).
[48]L. Huang, D. R. Chowdhury, S. Ramani, M. T. Reiten, S.-N. Luo, A. K. Azad, A. J. Taylor, and H.-T. Chen, Appl. Phys. Lett. **101**, 101102 (2012).
[49]P. A. George, W. Hui, F. Rana, B. G. Hawkins, A. E. Smith, and B. J. Kirby, Opt. Express **16**, 1577 (2008).
[50]L. Cong and R. Singh, preprint arXiv:1408.3711 (2014).